

OPTIMISATION OF NEON SXR (SOFT X-RAY) YIELD OF THE INTI PLASMA FOCUS MACHINE AT 12 kV

A. R. J. A. FEDERICO*, P. L. CHONG¹, S. H. SAW²

¹Centre for Plasma Research, Inti International University,
Persiaran Perdana BBN, Putra Nilai Negeri Sembilan, Malaysia

²Institute of Plasma Focus Studies, 32 Oakpark Drive, Chadstone, VIC3148, Australia

*Corresponding Author: federico.royjr@newinti.edu.my

Abstract

The INTI plasma focus machine is a 3 kJ Mather type plasma focus machine, powered by a single Maxwell capacitor. The system produces remarkable consistent focusing action in neon, making it a suitable source for the production of high energy photons, electrons, ions and neon soft x-rays (SXR). The aim of this paper is to optimise the neon SXR yield of the INTI plasma focus machine operated at 12 kV by parametrically, changing the anode dimensions (radius and length) using the Lee Model Code (version RADPFV5.15dd). Results of the optimisation procedures resulted in a neon SXR yield of 6.47 J at 2.5 torr and 12 kV, with a shorter length and a fatter anode radius of 7.9 cm and 1.2 cm respectively. This gives an improvement in the neon SXR yield of 40% when compared to neon SXR yield of 2.74 J at 2.5 torr 12 kV with the present configurations.

Keywords: INTI PF, Neon SXR, Neon SXR yield, Lee model code.

1. Introduction

The INTI plasma focus machine is a Mather type plasma focus machine and is one of the machines originally developed as the UNU/ICTP PFF (United Nations University/International Centre for Theoretical Physics Plasma Focus Facility). This machine is used for research and training to develop practical knowledge and skills in Plasma Physics, including fusion, in developing countries [1, 2]. The INTI plasma focus machine is a 3 kJ system powered by a single Maxwell capacitor switched by a parallel-plate swinging cascade air-gap. The system produces remarkably consistent focusing action in several gases including air, argon, hydrogen, helium, carbon dioxide, krypton and deuterium. Specifically, the INTI plasma focus machine is suitable for a good yield of neon SXR when neon

Nomenclatures	
A	Absorption factor
a	Anode radius
b	Cathode radius
C_0	Capacitor
f_c	Axial current factor
f_{cr}	Radial current factor
f_m	Axial mass swept-factor
f_{mr}	Radial mass factor
I_{peak}	Peak current
I_{pinch}	Pinch current
L_0	Inductor
M	Photonic excitation number
Ne	Neon
n_i	number density
P	Pressure
PF	Plasma Focus
Q_L	Line radiation
R_0	Resistor
r_p	Pinch radius
S	Speed factor
SG	Switch gap
SXR	Soft x-ray
T	Temperature
t	Time
UNU/IC	United Nations University/International Centre for Theoretical
$TP PFF$	Physics Plasma Focus
V_0	Input voltage
v_a	Axial velocity
v_p	Pinch velocity
v_s	Shock wave velocity
Y_{SXR}	Soft x-ray yield
Z	Effective charge number
Z_f	Pinch length
Z_n	Atomic number
z_0	Anode length

is used as a working gas [3]. The electric current is supplied by a 15 kV, 30 μ F capacitor. The external inductance is 110 nH. This machine is originally designed for neutron yield and has a speed factor of 97 kA/cm per [torr of deuterium]^{1/2} that is consistent with the range of other neutron-optimised plasma focus devices operating in deuterium [4]. The speed factor S is an indicator of the speeds in both the axial and radial phases. When operated in deuterium, the INTI plasma focus machine is designed for an average axial speed of 6 cm/ μ s running over an anode length of 16 cm. At this length, the axial run-down time matches the effective current rise time of 2.6 μ s at an end axial speed of nearly 10 cm/ μ s [1].

However, when the INTI plasma focus machine is operated in neon, Liu [3] and Bing [5] has shown that a focus pinch compression temperature of 200-500 eV is

suitable for a good yield of neon soft x-rays. This requires an end axial speed of 6-7 cm/ μ s, requiring an average speed of 4 cm/ μ s. Hence for time matching, the present INTI plasma focus machine has too long an anode which needs to be reduced by around 30%-40%. We used this consideration in our optimisation of the INTI plasma focus machine for neon operation. The numerical experiments will show that a drastic reduction in anode length is necessary. The same procedures were done by the authors in [6], whereby the recommended anode radius and length of 1.2 cm and 7cm at 14 kV. The optimised anode dimensions improved the neon SXR yield of the INTI plasma focus machine by three-folds.

2. Lee Model Code

The Lee Model Code couples the electrical circuit with plasma focus dynamics, thermodynamics and radiation, enabling realistic simulation of all gross focus properties. The code has been used extensively in several machines including UNU/ICTP PFF [1, 3-4, 7-8] NX1 [9], NX2 [4, 9-10] and has been adopted for the Filippov-type DENA [11]. A recent development is a template that shows the correlation of the neon SXR signal with the plasma focus dynamics [12] and the inclusion of the anomalous resistance phase to simulate the Type 2 high inductance plasma machine [13]. The Lee Model Code simulates the discharge evolution of the plasma dynamics shown in Fig. 1.

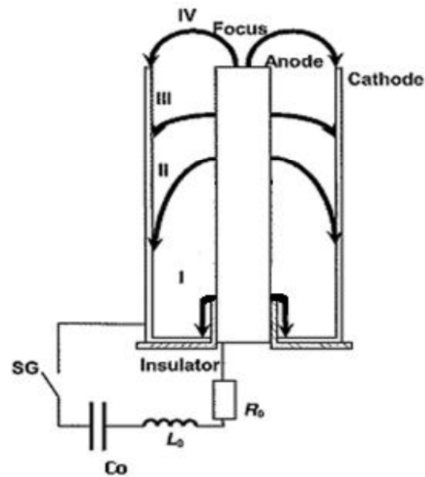


Fig. 1. The plasma focus with external capacitor C_0 , external inductance L_0 switch and the focus tube.

The discharge evolution consists of two main phases, the axial (I, II and III) and radial phase (IV). The axial phase starts with a breakdown phase (or inverse pinch). It refers to the electrical breakdown in a focus tube when a high voltage pulse is applied across the electrodes at an appropriate filling gas. An axial symmetric current sheath is formed at the end of this phase. This is followed by the axial acceleration phase (or axial rundown phase), whereby the current sheath is accelerated in the forward z-direction by the axial component of the Lorentz

force towards the open end of the anode. The axial phase ends when the current sheath reaches the open end of the anode. The radial phase then begins.

In the radial phase (or radial collapse phase) the current sheath implodes in a radially inward direction. The evolution of the radial is divided into four sub-phases (see Fig. 2), namely, the radial inward shock phase (curves 1-2 and 1-3), radial reflected shock phase (curves 2-3 and 3-4), slow compression (curve 4-5) and the expanded column radial phase (curve 5-6). In the radial inward shock phase, the plasma slug is formed (point 1), then the magnetic piston radius r_p and the shock front radius r_s decreases continually until $r_s=0$ (point 3). This is followed by the reflected shock phase. The final phase, the pinch phase (curve 4-5) plays an important role in the plasma focus evolution because of its extremely high energy density. When neon is used, the neon pinch is a source of neon SXR. Finally, the plasma focus decays in an expanded column phase (5-6) [14].

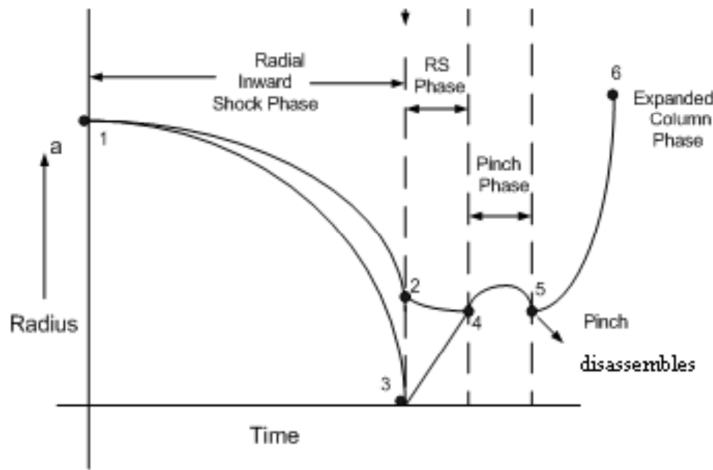


Fig. 2. The radial phase evolution.

The radial collapse phase plays the most important role in the plasma focus evolution due to its extremely high energy density and temperature. The focus pinch is a rich source of high energy particles and fusion products (when operated in deuterium) and also radiation such as soft X-rays. We note that the transition from slow compression (pinch phase) to the expanded column is observed in the laboratory to be in an extremely short time with plasma/current disruptions which resulted in localised regions of high densities and temperatures. These localised regions are not modelled in the code, which computes only average uniform density and temperature.

However, since the code incorporates four model parameters f_m and f_c (mass and current factors for the axial phase) and f_{mr} and f_{cr} (mass-swept-up and current factor in the radial phase) by fitting the computed to the measured total current waveform, the model incorporates the energy and mass balances equivalent to other processes which are not modelled. Therefore, the computed gross features such as speeds and trajectories and integrated neon SXR yields have been

extensively tested in numerical experiments for several machines and found to be comparable with measured values.

In the Lee Model Code [15], neon line radiation Q_L is calculated as follows:

$$\frac{dQ_L}{dt} = -4.6 \times 10^{-31} n_i^2 Z Z_n^4 (\pi r_p^2) Z_f / T \quad (1)$$

where, for the temperatures of interest in our experiments, we take the neon SXR yield $Y_{SXR} = Q_L$, where Z_n is the atomic number. Since in our code, is obtained by integrating over the pinch duration, the neon SXR energy generated within the plasma pinch depends on the following properties: number density, effective charge number Z , pinch radius, pinch length, and temperature T and pinch duration.

This generated energy is affected by plasma self-absorption which depends on density and temperature; the reduced quantity of energy is then emitted as the neon SXR yield. These effects are compensated in the model by computing the volumetric plasma self-absorption factor “A” derived from the photonic excitation number M which is a function of, Z and T . However in our range of operation, the numerical experiments show that the plasma self-absorption is not significant. It was pointed out by Liu [4], that the temperature around 300 eV is optimum for neon SXR production. Bing’s subsequent work [5] and our experience through numerical experiments suggest that around 2×10^6 K (below 200 eV) or even a little lower could be better. Hence, for neon SXR scaling, there is a range of temperature (T windows) suitable for efficient emission of neon SXR.

3. Numerical Experiments on Standard UNU/ICTP PFF

To start the numerical experiments, we select a discharge current trace of the INTI plasma focus machine taken with a Rogowski coil. The following bank tube and operation parameters are used:

- Bank: static inductance $L_0 = 110$ nH, $C_0 = 30$ μ F, and stray resistance $r_0 = 12$ m Ω .
- Tube: cathode radius $b = 3.2$ cm, anode radius $a = 0.95$ cm and anode length $z_0 = 16$ cm.
- Operation: voltage $V_0 = 12$ kV and pressure = 2.5 torr neon.

The computed total discharge current waveform is fitted to the measured. Fitting involves sequential variations in all the parameters such as f_m, f_c, f_{mr} and f_{cr} for the axial and radial phases. These parameters are sequentially varied until a visually acceptable fit between the measured and computed current trace is obtained. The following fitted model parameters are obtained: $f_m = 0.05, f_c = 0.7, f_{mr} = 0.2$ and $f_{cr} = 0.8$. These fitted values of the model parameters are then used for the computation of all the discharges at various pressures given in Table 1(a). In addition, Table 1(b) shows the measured neon SXR yield of the original anode dimensions of the INTI plasma focus machine.

It is shown in Table 1(a) the peak value of the total discharge current I_{peak} decreases with decreasing pressure. The reason is due to the increasing dynamic resistance (rate of change of plasma inductance dL/dt that gives rise to the dynamic resistance equivalent to $0.5 dL/dt$) which is caused by the increasing

current-sheath speed when pressure is decreased. However, we can see that as pressure decreases, the pinch current I_{pinch} that flows through the pinched plasma increases. This is due to the shifting of the pinch time closer and closer toward the time of peak current as the current moves faster and faster. Even at the lowest pressure of 1 torr, the current sheet (with a peak axial speed of 8.3 cm/ μ s) is still less than for best matching and reaches the end of the anode just after the peak of the circuit current (which peaks at 2.6 μ s, a little earlier than the unloaded rise time). For the INTI plasma focus machine with original anode length of 16 cm, the operating pressure has to be around 0.9 torr in neon for the current sheath to reach the end of the anode at peak total current. Below 0.9 torr, the I_{pinch} starts to decrease as the pinch time now occurs before the current peak time. As the pressure decreases, the increase in I_{pinch} increases the neon SXR yield, at the same time decreases the number density as well. The interaction of the decrease in the number density will decide on the actual neon SXR yield versus pressure behaviour as shown in the computed results.

Table 1(a). Numerical neon SXR yield versus P for the INTI plasma focus machine with $L_0 = 110$ Nh, $C_0 = 30$ μ F, and RESF = 0.2, operating at 12 kV, using a combination of $Z_0 = 16$ cm, $A = 0.95$ cm with $B = 3.2$ cm.

P (torr)	I_{peak} (kA)	I_{pinch} (kA)	Peak v_a (cm/ μ s)	Numerical neon SXR Data				S (kA/(cm[torr Ne] ^{1/2}))	neon SXR (J)
				T_{pinch} $\times 10^6$ (K)	Peak v_s (cm/ μ s)	Peak v_p (cm/ μ s)			
4.5	151.7	72.8	5.1	0.69	12.7	10.2	75.3	0.15	
4	150.4	80.9	5.6	0.97	14.7	11.6	79.2	0.42	
3.5	148.7	88.0	6.4	1.31	17.0	12.9	83.7	1.09	
3	147.8	90.8	6.8	1.94	21.0	14.5	89.8	2.69	
2.5	147.0	92.3	7.1	2.01	21.3	14.7	97.9	2.68	
2	146.0	94.0	7.5	2.6	24.8	15.5	108.7	1.08	
1.5	144.5	95.3	8.1	3.41	25.5	16.6	124.2	0.45	
1	144.2	95.2	8.3	4.74	27.8	18.7	151.8	0.14	

Table 1(b). Measured neon SXR versus P of the INTI plasma focus machine.

P (torr)	neon SXR (J)	Error range \pm (J)
4.5	0.144	0.03
4	0.876	0.31
3.5	1.082	0.5
3	3.05	1.04
2.5	3.096	0.99
2	2.552	0.31
1.5	0.97	0.30
1	0.144	0.04

There are two major factors determining the characteristic neon SXR yield. The temperature has to be within a certain window (200-500 eV) in order that most of the neon ions are 8th and 9th ionised. These are the He-like and H-like neon ionic states that emit the neon SXR [12]. The appropriate end axial speed is

6-7 cm/ μ s which then, in the geometry of the INTI plasma focus machine generate the appropriate radial on-axis speed of close to 20 cm/ μ s. This radial on-axis speed produces the correct pinch temperature within the window.

The second factor is the density since the radiation yield is proportional to the relevant density squared. Thus at too low a pressure the density of the ions is low and at the same time the temperature may be too high whilst at too high a pressure the density of the ions would be high, however the temperature may be too low, below the temperature window. Thus there may be found an operational pressure at which the temperature is within the window whilst the density is still high enough. That could be the pressure that gives the optimum neon SXR yield.

To validate the numerical experiments, we run the experiments on the INTI plasma focus machine. Neon SXR measurements were obtained using a five-channel pin neon SXR detector. The 5-channel filtered diode SXR spectrometer is used. This includes 2-channel characteristic Neon SXR detector, one channel is filtered by 13 μ aluminium film and a second filter by 125 μ mylar + 3 μ aluminium film. This combination has been designed so that any difference signal indicates detection of SXR within the spectral window of 900-1550 eV photonic energy (equivalent to 8-14 A) which falls the range of characteristic lines emitted by H-like and He-like neon ions.

Comparing computed with measured neon SXR yields (Fig. 3) the result shows reasonable agreement. The differences are as follows. The measured optimum point is at 2.5 torr and has a neon SXR yield of 3.096 J. This compares with the numerical optimum pressure of 3 torr with corresponding neon SXR yield of 2.7 J. Both numerical and measured SXR yield shows similar trend. As pressure increases, the pinch temperature goes from high to low. At lower pressure, temperature is too high to produce significant neon SXR, at around 2.5 torr, the temperature optimised the SXR yield. As the pressure continue to increase, the temperature decreases and subsequently lower the SXR yield. The decrease in SXR yields as the pressure increases are due to decrease in plasma speed and the increase in the duration of axial speed. The Lee model code provides good guidelines in analysing SXR yield even an experimental data are not possible.

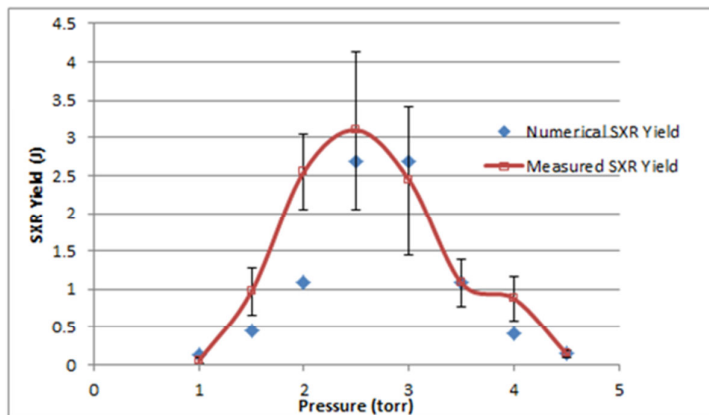


Fig. 3. Measured and computed neon SXR yield of INTI plasma focus machine at different pressures.

4. Optimising for a Practical Optimum Configuration.

Numerical analysis using the Lee Model Code was carried out to determine the optimum configuration for the electrodes using the INTI plasma focus machine. The operating parameters were retained at 12 kV in Neon with $L_0= 110$ nH, $C_0= 30$ μ F. The model parameters were also retained at $f_m= 0.05$, $f_c= 0.7$, $f_{mv}=0.2$, and $f_{cv}=0.8$. The value of b is kept constant at 3.2 cm. The pressure (P), anode length (z_0), and anode radius (a) were parametrically varied and the results were tabulated in Table 2.

Preliminary optimisation results shows that there are two sets of values that give an optimum neon SXR yield ($a = 1.4$ cm, $z_0 = 7$ cm) at $P = 1.6$ torr and ($a = 1.2$ cm, $z_0 = 9$ cm) at $P = 2.2$ torr (Fig. 4). As shown in Fig. 4, both anode radius and anode length were varied to optimised SXR yield. Anode radius affects the plasma pinch while anode length affects the plasma speed which affects the SXR yield. As shown in Fig. 4, SXR yield increases as the anode length increases while the anode length decreases. Since the SXR yield is optimised, the temperature window for neon SXR is considered and hence it resulted to the sudden drop off on the right side of each set of values (both anode radius and length).

Numerical experiments were continued to optimise the neon SXR yield for a fix anode length $z_0 = 7$ cm, $P = 1.6$ torr, while anode “a” is parametrically change (starting at a =1.4 cm) while taking note of the pinch temperature of 2.3×10^6 K. The result is shown in Fig. 5. The maximum neon SXR yield is 4.41 J at $a = 1.407$ cm. Next, the anode length is fixed at 1.407 cm, $z_0 = 7$ cm, while the pressure is parametrically varied while taking note of the pinch temperature of 2.3×10^6 K.

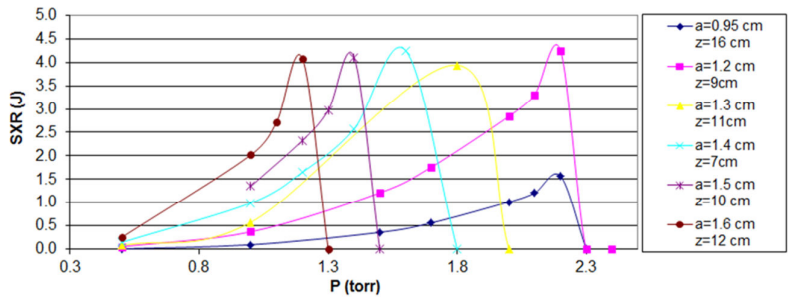


Fig. 4. Optimum SXR yield at different pressures and different anode dimensions.

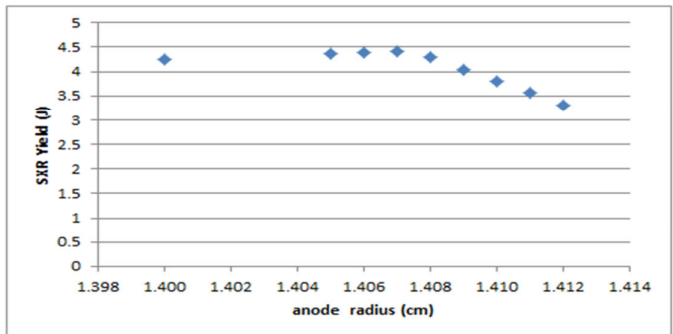


Fig. 5. Optimum neon SXR yield at fix anode length $z_0 = 7$ cm and $P=1.6$ torr while anode radius is parametrically varied.

Table 2. Computed neon SXR yield versus P for optimised INTI plasma focus machine.

a (cm)	z_0 (cm)	P_0 (torr)	I_{peak} (kA)	I_{pinch} (kA)	peak V_a (cm/ μ s)	peak V_s (cm/ μ s)	peak V_p (cm/ μ s)	S (kA/(cm[torr Ne] ^{1/2}))	neon SXR (J)
1.4	7	0.5	130.48	101.23	8.09	28.03	19.02	131.80	0.15
		1	145.23	111.93	6.5	25.3	16.43	103.74	0.99
		1.2	148.77	114.38	6.13	24.92	15.95	97.01	1.65
		1.4	151.43	116.15	5.82	24.77	15.53	91.42	2.57
		1.6	153.48	117.46	5.56	23.18	15.09	86.67	4.25
		1.8	155.20	118.38	5.33	21.8	14.73	82.63	0
		2	156.61	117.69	5.19	22	14.82	84.24	0
1.2	9	0.5	134.49	104.27	9.03	32.01	22.65	158.50	0.06
		1	147.7	113.81	7.19	26.95	17.98	123.08	0.37
		1.5	153.27	117.23	6.23	25.34	16.42	104.29	1.21
		1.7	154.46	117.9	5.94	25.02	16.03	98.72	1.76
		2	155.57	118.18	5.58	24.57	15.49	91.67	2.84
		2.1	155.86	118.11	5.48	24.3	15.31	89.63	3.31
		2.2	156.12	118	5.37	23.21	15.14	87.71	4.25
		2.3	156.37	117.86	5.28	22.6	14.97	85.92	0

The result is shown in Fig. 6. The maximum neon SXR yield at this point is 4.44 J at P of 1.601 torr. Numerical experiments were done for the second set of optimum neon SXR value of $a = 1.2$ cm and $z_0 = 9$ cm. Following the same parametrical INTI plasma focus machine previous dimensions, the result is shown in Fig. 7. The optimum neon SXR yield of 4.65 J was obtained at $a = 1.2$ cm, $z_0 = 7.9$ cm and a pressure of 2.255 torr.

Finally, to compare the neon SXR yield of the new anode dimensions with the original dimensions, another numerical experiment were ran without considering the temperature window for neon SXR. This time the new anode dimensions $a = 1.2$ cm $z_0 = 7.9$ cm were used. The pressure was varied from 1 to 4.5 torr. As discussed in previous section, the SXR yield is related to plasma temperature, density and particles in the plasma column. At the low pressure, the plasma temperature is too high and fewer particles are collected into x-ray radiative plasma column, therefore the x-ray yield is low. If the pressure is too high, the plasma temperature will be too low to give good SXR yield. An optimum SXR yield occurs at a pressure of 2.5 torr. As we can see in Fig. 8, there was an improvement of neon SXR yield from 2.74 J to 6.47 J. This experimental exercise resulted in a 2.5 fold increase in neon SXR yield.

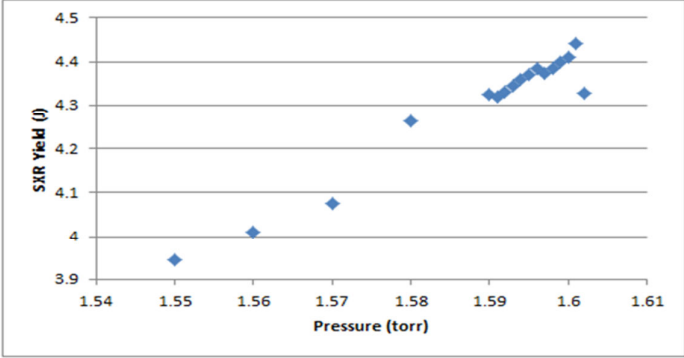


Fig. 6. Optimum neon SXR yield at fix anode length z_0 and anode radius = 1.407 cm while pressure P is parametrically varied.

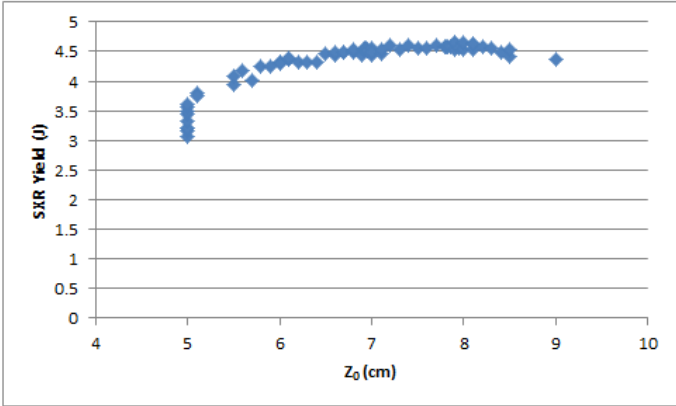


Fig. 7. Optimum neon SXR Yield at fix anode radius $a = 1.2$ cm while pressure P and length z_0 were parametrically varied.

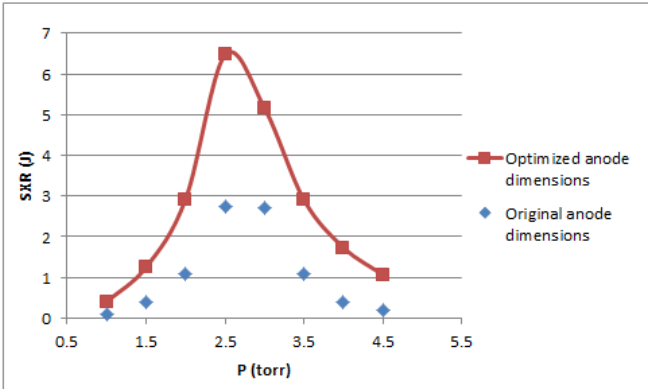


Fig. 8. Comparison of computed neon SXR yield of the new anode dimensions ($a = 1.2$, $z_0 = 7.9$ cm) with the existing anode dimensions ($a = 0.95$ cm, $z_0 = 16$ cm).

5. Conclusions

An optimisation exercise using the Lee Model code was done. By shortening the anode length z_0 from 16 cm to 7.9 cm and increasing the anode radius “a” from 0.95 to 1.2 cm, it is predicted that an optimum SXR yield of 6.47 J can be obtained. In addition, there is a good agreement in trend between the numerical and measured SXR yield of the INTI plasma focus machine at operated at 12 kV.

References

1. Lee, S.; Tou, T.Y.; Moo, S.P.; Eissa, M.A.; Gholap, A.V.; Kwek, K.H.; Mulyodrono, H.; Smith, A.J.; Suyadi, S.; Usada, W.; and Zakaullah, M. (1988). A simple facility for the teaching of plasma dynamics and plasma nuclear fusion. *American Journal of Physics*, 56(1), 62-68.
2. Lee, S.; and Wong, C.S. (2006). Initiating and strengthening plasma research in developing countries. *Physics Today*, 29(5), 31-36.
3. Liu, M. (2006). *Soft X-rays from compact plasma focus*. Ph.D. Dissertation, Nanyang Technological University, Singapore.
4. Lee, S.; and Serban, A. (1996). Dimensions and lifetime of the plasma focus pinch. *IEEE Transaction on Plasma Science*, 24(3), 1101-1105.
5. Bing, S. (2000). *Plasma dynamics and X-ray emission of the plasma focus*, Ph.D. Dissertation, Nanyang Technological University, Singapore.
6. Saw, S.H.; Lee, P.; Rawat, R.S.; and Lee, S. (2009). Optimising UNU/ICTP PFF plasma focus for neon soft X-ray operation. *IEEE Transaction on Plasma Science*, 37(7), 1276-1282.
7. Lee, S. (1998). *In twelve years of UNU/ICTP PFF- A Review*, Trieste, Italy: Abdus Salam ICTP, (5-34).
8. Sprngham, S.V.; Lee, S.; and Rafique, M.S. (2000). Correlated deuteron energy spectra and neutron yield for a 3 kJ plasma focus. *Plasma Physics Control Fusion*, 42(10), 1023-1032.
9. Lee, S.; Lee, P.; Zhang, G.; Patran, A.; Feng, X.; Gribkov, V.A.; Liu, M.; Serban, A.; and Wong, T. (1998). High rep rate high performance plasma focus as a powerful radiation source, *IEEE Transaction on Plasma Science*, 26(4), 1119-1126.
10. Wong, D.; Lee, P.; Zhang, T.; Patran, A.; Tan, T.L.; Rawat, R.S.; and Lee, S. (2007). An improved radiative plasma focus model calibrated for neon-filled NX2 using tapered anode. *Plasma Sources Science Technology*, 16(1), 116-123.
11. Sialpoush, V.; Tafreshi, M.A.; Sobhanian, S.; and Khorram, S. (2005). Adaptation of Sing Lee’s model to the Filippov type plasma focus geometry. *Plasma Physics Control Fusion*, 47(7), 1065-1075.
12. Lee, S.; Saw, S.H.; Rawat, R.S.; Lee, P.; Talebitaher, A.; Abdou, A.E.; Chong, P.L.; Roy Jr, F.A.; Singh, A.; Wong, D.; and Devi, K. (2011). Correlation of measured soft x-ray pulses with modelled dynamics of the plasma focus. *IEEE Transactions on Plasma Science*, 39(11), 3196-3202.

13. Lee, S.; Saw, S.H.; Abdou, A.E.; and Torreblanca, H. (2011). Characterizing plasma focus devices-role of the static inductance-instability phase fitted by anomalous resistances. *Journal of Fusion Energy*, 30(4), 277-282.
14. Roy Jr, F.A.; Chong, P.L.; Saw, S.H.; and Lee, S. (2010). Generation of soft X-Ray from plasma focus machine. *International Journal of Engineering and Technology*, 1(1) (Electronic Version), http://ijeat.newinti.edu.my/Journal%20Paper/Vol%201/Issue%201/IJEAT_Vol1_No1_3.pdf.
15. Lee, S. (2013). Radiative dense plasma focus computation package: RADF. Retrieved March 5, 2013 from <http://www.intima.edu.my/school/fas/UFL/File1RADPF.htm>.